

# Structural Characterization of the Type-III Pilot-Secretin Complex from *Shigella flexneri*

Mark Okon,<sup>1,2,6</sup> Trevor F. Moraes,<sup>1,6</sup> Paula I. Lario,<sup>1</sup> A. Louise Creagh,<sup>3,4</sup> Charles A. Haynes,<sup>3,4,5</sup> Natalie C.J. Strynadka,<sup>1,3,5,\*</sup> and Lawrence P. McIntosh<sup>1,2,3,\*</sup>

<sup>1</sup>Department of Biochemistry & Molecular Biology

<sup>2</sup>Department of Chemistry

<sup>3</sup>Michael Smith Laboratories

<sup>4</sup>Department of Chemical and Biological Engineering

<sup>5</sup>Centre for Blood Research

University of British Columbia, Vancouver, BC V6T 1Z3, Canada

<sup>6</sup>These authors contributed equally to this work

\*Correspondence: natalie@byron.biochem.ubc.ca (N.C.J.S.), mcintosh@chem.ubc.ca (L.P.M.)

DOI 10.1016/j.str.2008.08.006

## SUMMARY

Assembly of the type-III secretion apparatus, which translocates proteins through both membranes of Gram-negative bacterial pathogens into host cells, requires the formation of an integral outer-membrane secretin ring. Typically, a small lipidated pilot protein is necessary for the stabilization and localization of this ring. Using NMR spectroscopy, we demonstrate that the C-terminal residues 553–570 of the *Shigella flexneri* secretin MxiD encompass the minimal binding domain for its cognate pilot MxiM. Although unstructured in isolation, upon complex formation with MxiM, these residues fold into an amphipathic turn-helix motif that caps the elongated hydrophobic cavity of the cracked  $\beta$ -barrel pilot. Along with a rearrangement of core aromatic residues, this prevents the binding of lipids within the cavity. The mutually exclusive association of lipids and MxiD with MxiM establishes a framework for understanding the role of a pilot in the outer-membrane insertion and multimerization of the secretin ring.

## INTRODUCTION

Shigellosis, an infectious disease caused by various species of *Shigella*, is responsible for over one million deaths per year worldwide, and is particularly lethal for young children and the elderly (Kotloff et al., 1999). Similar to other Gram-negative pathogens, including enterohemorrhagic and enteropathogenic *Escherichia coli*, *Salmonella*, *Yersinia*, *Chlamydia*, and *Pseudomonas*, *Shigella* invades host organisms with a specialized apparatus called the type III secretion system (T3SS). This pathogen-specific multiprotein complex delivers virulence proteins from the bacterium through a hollow tube that traverses both the inner and outer bacterial membranes and the host cell membrane (Blocker et al., 2001). The T3SS is essential for colonization of these pathogens in the epithelial cells of the host intestinal mucosa, and thus represents a key target for the design of antimicrobials.

Assembly of the T3SS requires the initial formation of an outer-membrane component from the secretin protein superfamily (Thanassi and Hultgren, 2000). Once transported to the periplasm, monomeric secretins associate into large and highly stable oligomeric pores of 12–14 subunits. Electron microscopy studies have shown that several secretin family members from apparently unrelated protein secretion pathways, including the T3SS, the type-II secretion system (T2SS), and the type-IV pilus biogenesis pathway, all form ring-like structures with an internal diameter large enough to allow for the passage of unfolded or partially unfolded proteins through these outer-membrane gateways (Linderoth et al., 1997; Nouwen et al., 1999; Koster et al., 1997; Burghout et al., 2004b; Collins et al., 2004).

Stabilization, oligomerization, and membrane association of secretins generally involves the presence of a small conjugate protein called a pilot (Thanassi and Hultgren, 2000). Secretin pilots have a characteristic signal peptide leader sequence with an additional conserved cysteine in a lipidation sequence motif (Hayashi and Wu, 1990). This cysteine has been shown to be lipid modified for a number of characterized pilots, including MxiM, PulS, OutS, YscW, and InvH (Allaoui et al., 1992; Hardie et al., 1996; Daefler and Russel, 1998; Schuch and Maurelli, 1999; Shevchik and Condemine, 1998; Burghout et al., 2004a). However, beyond the lipidation motif, there is little sequence similarity between pilots (<15%), whereas secretin family members show significantly higher sequence conservation (~30%) (Genin and Boucher, 1994; Shevchik and Condemine, 1998; Daefler and Russel, 1998; Schuch and Maurelli, 2001; Lario et al., 2005). Indeed, even among T3SS-specific pilots, there are considerable variations to their predicted charges and secondary structures. This may not be surprising, considering that pilots bind to the sequence-divergent C-terminal ends of secretins (Daefler et al., 1997; Burghout et al., 2004a).

The recently determined structure of the T3SS pilot MxiM from *Shigella* (Lario et al., 2005) reveals the presence of an elongated hydrophobic cavity for the binding of lipids. The cavity is shaped by a curved  $\beta$  sheet related to the eight stranded  $\beta$ -barrel lipocalins (Flower et al., 2000). The precise functional role of this hydrophobic cavity is not clear. Similar to the well-known lipocalin family members, such as PagP (Ahn et al., 2004), the *Shigella* pilot MxiM is capable of binding hydrophobic detergents or lipids, with C16 acyl variants appearing to fit the cavity in an

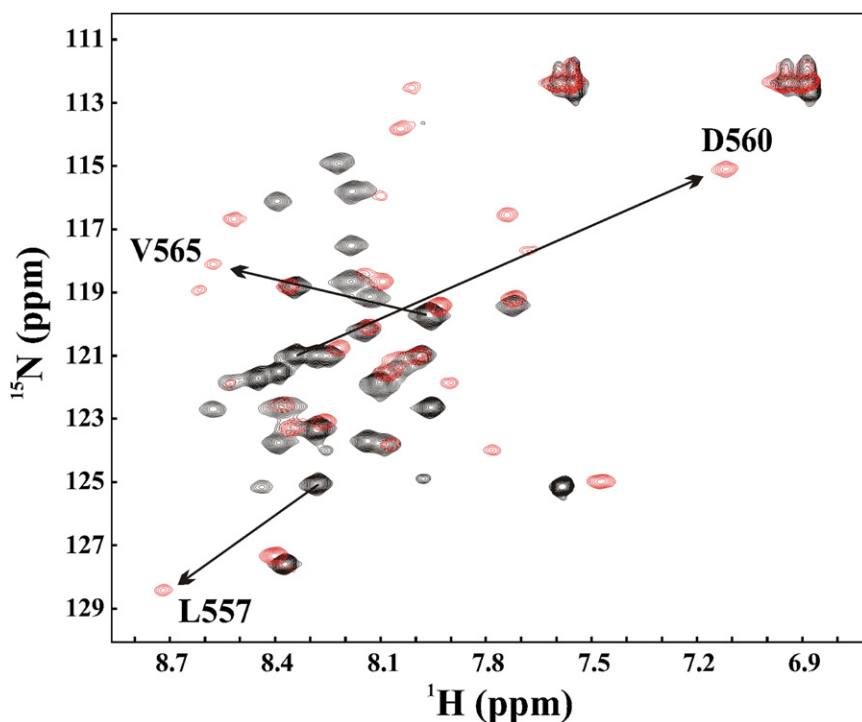


**Figure 1. Identification of the Residues within MxiD<sup>525–570</sup> that Mediate Binding to MxiM<sup>28–142</sup>**

Shown are the superimposed <sup>15</sup>N-HSQC spectra of <sup>15</sup>N/<sup>13</sup>C-labeled MxiD<sup>525–570</sup> in the absence (black) and presence (red; molar ratio 1:1.3) of excess unlabeled MxiM<sup>28–142</sup>. For clarity, only signals from three amides in both states are labeled.

Upon titration with MxiM<sup>28–142</sup>, a new and well-dispersed set of signals were observed in the <sup>15</sup>N-HSQC spectrum of the secretin fragment MxiD<sup>525–570</sup> (Figure 1). These signals arose in the slow exchange regime, indicative of tight binding on the chemical shift time scale. Assignment of the spectrum of the bound polypeptide revealed that the dispersed signals were from its C-terminal ~18 residues (Figures 1 and 2B). Based upon its main chain chemical shifts, as well as sequential interresidue <sup>1</sup>H-<sup>1</sup>H NOE interactions, MxiM<sup>28–142</sup> binding induced these residues to adopt an extended conformation followed by  $\alpha$ -helical structure

(Figure 2C). In contrast, the N-terminal ~28 amides of MxiD<sup>525–570</sup> were unperturbed by the presence of the pilot protein, and remained predominantly disordered, albeit with some helical propensity. <sup>15</sup>N relaxation measurements supported this conclusion, as the amides within the bound portion of the secretin fragment had heteronuclear <sup>1</sup>H-<sup>15</sup>N NOE values greater than 0.6, indicative of a stable structure on the nanosecond-to-picosecond time scale, as well as an effective correlation time for global tumbling of 10.7 ns, as expected for an ~13 kDa complex at 15°C (Figure 2D). The N-terminal portion of MxiD<sup>525–570</sup> exhibited lower heteronuclear NOE values and, hence, greater, albeit not unrestricted, flexibility on this fast time scale, confirming that it does not directly contact MxiM<sup>28–142</sup>.

optimal manner (Lario et al., 2005). Importantly, isothermal titration calorimetry (ITC) studies have revealed that lipid access to the hydrophobic cavity of MxiM is impaired by the binding of a peptide corresponding to the C-terminal residues 525–570 of its cognate secretin MxiD (Lario et al., 2005). To understand further the role of pilot/secretin complexes in T3SS formation, we have used NMR spectroscopy and ITC to characterize the structural and thermodynamic bases for the mutually exclusive interactions of lipids and the secretin MxiD with the pilot MxiM. Upon binding its cognate pilot, the disordered C terminus (residues 553–570) of MxiD folds as a turn-helix motif that lies across the open end of the MxiM barrel. Along with a rearrangement of its core aromatic side chains, the presence of this MxiD “lid” prevents the binding of lipids within the hydrophobic cavity of MxiM. Based on these results, we propose a model for the *in vivo* localization of the lipidated-MxiM/MxiD complex to the outer membrane via the Lol lipoprotein trafficking system.

## RESULTS

### Residues 553–570 of MxiD<sup>525–570</sup> Become Structured Upon Binding MxiM<sup>28–142</sup>

Previously, an expressed peptide, MxiD<sup>525–570</sup>, corresponding to the C-terminal 46 residues of MxiD, was shown by ITC to bind MxiM<sup>28–142</sup> *in vitro* (Lario et al., 2005). In order to better define this interaction, we used NMR spectroscopy to characterize MxiD<sup>525–570</sup> free and bound to the pilot protein. The <sup>15</sup>N-HSQC spectrum of isolated MxiD<sup>525–570</sup> had poorly resolved amide <sup>1</sup>H<sup>N</sup> chemical shifts, diagnostic of a predominantly unstructured polypeptide (Figure 1). However, based on analysis of its assigned main chain <sup>1</sup>H, <sup>15</sup>N, and <sup>13</sup>C chemical shifts, residues 529–541 appeared to transiently adopt a helical conformation (Figure 2A).

(Figure 2C). In contrast, the N-terminal ~28 amides of MxiD<sup>525–570</sup> were unperturbed by the presence of the pilot protein, and remained predominantly disordered, albeit with some helical propensity. <sup>15</sup>N relaxation measurements supported this conclusion, as the amides within the bound portion of the secretin fragment had heteronuclear <sup>1</sup>H-<sup>15</sup>N NOE values greater than 0.6, indicative of a stable structure on the nanosecond-to-picosecond time scale, as well as an effective correlation time for global tumbling of 10.7 ns, as expected for an ~13 kDa complex at 15°C (Figure 2D). The N-terminal portion of MxiD<sup>525–570</sup> exhibited lower heteronuclear NOE values and, hence, greater, albeit not unrestricted, flexibility on this fast time scale, confirming that it does not directly contact MxiM<sup>28–142</sup>.

### MxiD<sup>553–570</sup> Binds MxiM<sup>28–142</sup> with High Affinity

Our initial NMR studies demonstrated that the interaction between MxiM and MxiD is dependent upon the C-terminal ~18 amino acids of the secretin. Accordingly, we obtained a synthetic peptide, MxiD<sup>553–570</sup>, corresponding to this minimal binding sequence. Based on ITC measurements, MxiD<sup>553–570</sup> binds MxiM<sup>28–142</sup> in a 1:1 stoichiometry ( $n = 0.77$ ), and with a  $K_a$  of  $1.4 (\pm 0.5) \times 10^7 \text{ M}^{-1}$  at 25°C. This is very comparable to the  $K_a$  of  $1.1 (\pm 0.3) \times 10^7 \text{ M}^{-1}$  determined previously for MxiD<sup>525–570</sup> (Lario et al., 2005), confirming that residues 553–570 encompass the MxiM-recognition sequence of MxiD.

The NMR spectra of MxiM<sup>28–142</sup> are well dispersed, and have assigned <sup>1</sup>H, <sup>13</sup>C, and <sup>15</sup>N signals consistent with its cracked  $\beta$ -barrel secondary structure (data not shown). Upon titration with unlabeled MxiD<sup>553–570</sup>, the <sup>15</sup>N-HSQC spectrum of <sup>15</sup>N-labeled MxiM<sup>28–142</sup> also changed dramatically in the slow exchange regime to yield that of the MxiM<sup>28–142</sup>/MxiD<sup>553–570</sup> complex (Figure 3). An initial mapping of the amide chemical shift perturbations due to MxiD<sup>553–570</sup> binding onto the crystal structure of

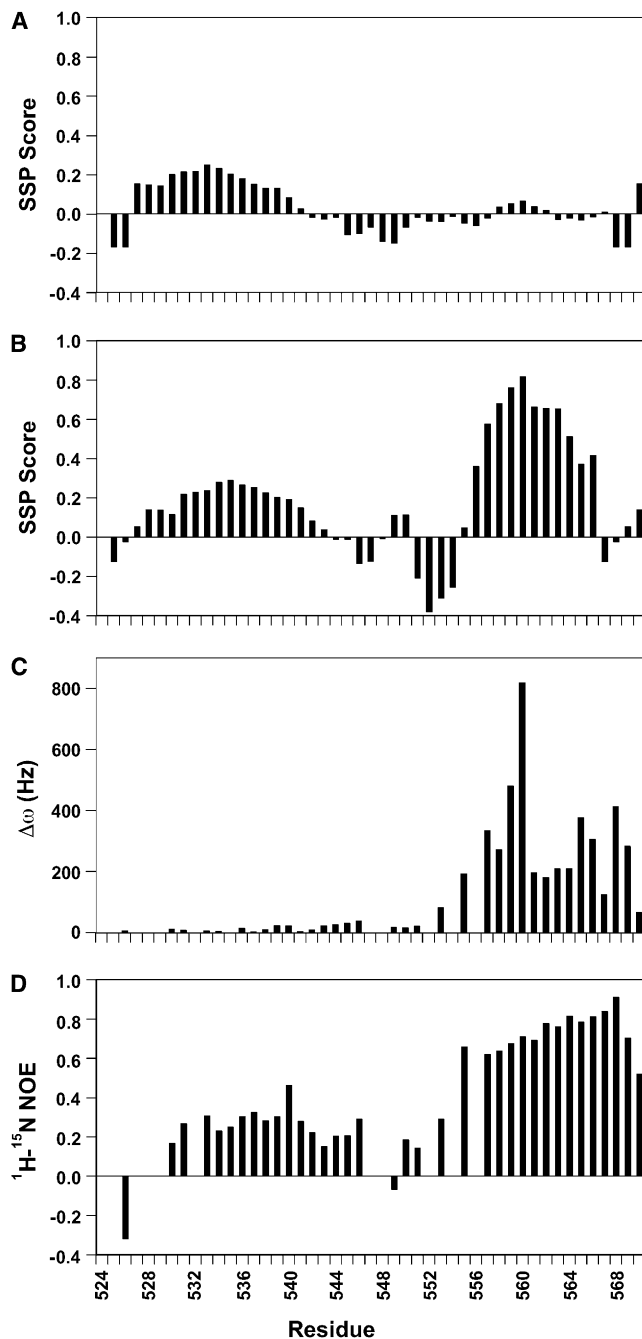


**Figure 2. Residues 553–570 of MxiD<sup>525–570</sup> Become Structured upon Binding MxiM<sup>28–142</sup>**

(A) An analysis of the main chain chemical shifts of MxiD<sup>525–570</sup> with the SSP algorithm (Marsh et al., 2006) reveals that the free polypeptide is predominantly unstructured, albeit with residues 529–541 transiently adopting helical conformations.

(B) In contrast, binding to MxiM<sup>28–142</sup> induces the C-terminal ~18 residues of MxiD<sup>525–570</sup> to adopt an extended conformation followed by a helical conformation. SSP scores from 0 to +1 indicate increasing  $\alpha$ -helical structure, whereas those from 0 to –1 correspond to increasing  $\beta$ -strand structure.

(C) Amide chemical shift perturbations ( $\Delta\omega = [(\Delta\omega_{1H})^2 + (\Delta\omega_{15N})^2]^{1/2}$  in Hz, recorded with a 600 MHz spectrometer) of MxiD<sup>525–570</sup> in the presence versus the absence of MxiM<sup>28–142</sup> also show that only residues ~553–570 undergo spectral, and hence, structural changes upon pilot binding.

free MxiM<sup>28–142</sup> revealed extensive changes, both near the open end of the  $\beta$  barrel and within its hydrophobic cavity. Due to these extensive spectral changes, the binding interface for MxiD<sup>553–570</sup> could not be readily identified, and concern arose as to whether the structure of peptide-bound MxiM<sup>28–142</sup> might differ significantly from that of its detergent-bound state, as defined by X-ray crystallography (Lario et al., 2005). Therefore, we used NMR spectroscopy to determine directly the structure of the MxiM<sup>28–142</sup>/MxiD<sup>553–570</sup> complex without introducing any bias from docking or other modeling approaches.

### Structure of the MxiM<sup>28–142</sup>/MxiD<sup>553–570</sup> Complex

The structural ensemble of the MxiM<sup>28–142</sup>-MxiD<sup>553–570</sup> complex was determined from an extensive set of NMR-derived distance restraints (Table 1; Figure 4). Peptide-bound MxiM<sup>28–142</sup> retained the previously described secondary and tertiary structure of the free pilot protein, with eight antiparallel  $\beta$  strands (strand A, residues 36–40; B, 52–57; C, 62–67; D, 71–79; E, 82–90; F, 116–117; G, 126–130; H 133–138) forming a pseudobarrel, “cracked” on one side by a  $3_{10}$  helix (43–45) and an  $\alpha$  helix (99–114). The barrel is closed on one end by a disulfide bridge, yet open on the other, exposing a deep, hydrophobic cavity. Thus, despite rather extensive chemical shift perturbations upon MxiD<sup>553–570</sup> binding, the NMR-derived structural ensemble of MxiM<sup>28–142</sup> in complex closely resembles that of the free protein determined by X-ray crystallography. The root-mean-square deviation (rmsd) between the two is  $2.85 \pm 0.07 \text{ \AA}$  and  $1.66 \pm 0.03 \text{ \AA}$  for all main chain atoms and for those in  $\beta$  strands/ $\alpha$  helices, respectively. Indeed, the most significant change in the backbone conformations of the two structures was the outward displacement of the exposed loop L5 (named according to Lario et al. [2005]) between strands F and G to accommodate MxiD<sup>553–570</sup>.

MxiD<sup>553–570</sup> lies across the open end of the MxiM<sup>28–142</sup> barrel (Figure 4; see Figure S1 available online). As indicated by the initial chemical shift analysis of pilot-bound MxiD<sup>525–570</sup>, the secretin peptide folds as an  $\alpha$  helix (residues 561–568) preceded by an extended segment. The helix is amphipathic, such that residues Glu561, Leu564, Val565, Tyr567, and Leu568 interact with Trp36, Phe56, Tyr76, Phe78, Phe83, Leu117, and Ile126 at the top of the MxiM<sup>28–142</sup> hydrophobic cavity. The extended portion of MxiD<sup>553–570</sup> also provides contacts from Thr555, Thr556, Leu557, Leu558, and Glu559 to Gly81, Val116, Leu117, Lys118, G119, Ile126, and Leu127 of MxiM<sup>28–142</sup>. Although these contacts involve primarily hydrophobic side chains, they are flanked by a striking arrangement of electrostatic interactions. Namely, Lys118, Lys61, and Lys34 form a “triangle” around the open end of MxiM<sup>28–142</sup>, positioned to ion pair with the carboxyl groups of Glu559 in the extended region, Glu561 at the start of the  $\alpha$  helix, and Tyr570 at the C terminus of MxiD<sup>553–570</sup>, respectively. It is also noteworthy that residues 555–557 of MxiD<sup>553–570</sup>

(D) Heteronuclear  $^1\text{H}$ - $^{15}\text{N}$  NOE values for complexed MxiD<sup>525–570</sup> confirm that the C-terminal residues of the secretin fragment are well ordered when bound to MxiM<sup>28–142</sup>, whereas the remainder of the polypeptide is more conformationally mobile on the nanosecond to picosecond time scale. Decreasing NOE values are indicative of increased flexibility on this fast time scale. The data were obtained with  $^{13}\text{C}/^{15}\text{N}$ -labeled MxiD<sup>525–570</sup> and unlabeled MxiM<sup>28–142</sup>. Missing points correspond to prolines or residues with unassigned signals.

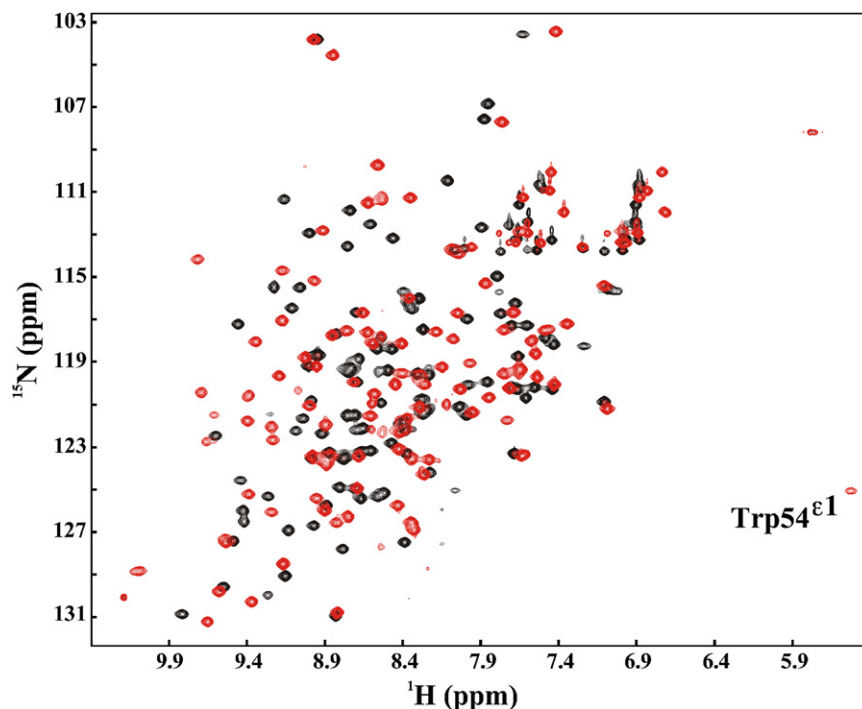


**Figure 3. The  $^{15}\text{N}$ -HSQC Spectrum of Free  $^{15}\text{N}/^{13}\text{C}$ -labeled MxiM $^{28-142}$  Becomes Extensively Perturbed upon Addition of Excess Unlabeled MxiD $^{553-570}$**

As shown in Figure 4, these changes are attributed to structural perturbations due to both MxiD $^{553-570}$  (black, apo MxiM $^{28-142}$ ; red, 1:1.3 molar ratio of MxiD $^{553-570}$ ) binding and DM displacement. For clarity, only the dramatically upfield-shifted signal from the indole  $^{15}\text{N}^{\epsilon 1}\text{H}$  of Trp54 in bound MxiM $^{28-142}$  (red) is labeled.

#### **MxiD $^{553-570}$ Excludes Binding of Detergents by MxiM $^{28-142}$**

Although the backbone structure of MxiM $^{28-142}$  does not change significantly upon association with MxiD $^{553-570}$ , the  $^{15}\text{N}$ -HSQC spectrum of the pilot protein was dramatically altered (Figure 3). Mapping the main chain chemical shift perturbations onto the structure of the complex revealed that changes occur both at the open end of the MxiM $^{28-142}$  barrel, as well as throughout its hydrophobic cavity (Figures 5A and 5B). Shift perturbations

lie in an extended conformation, antiparallel to the small  $\beta$  strand F (residues 116–117) of MxiM $^{28-142}$ . Although not well defined due to the absence of any experimentally determined hydrogen bonding restraints, this is suggestive of MxiD contributing an additional strand to the  $\beta$ -sheet structure of MxiM. Together, these interactions bury  $\sim 750^2$  and  $\sim 850 \text{ \AA}^2$  of accessible surface from MxiM $^{28-142}$  and MxiD $^{553-570}$ , respectively, and involve all but six residues (Ser553 and Glu554 at its flexible N terminus, Lys562, Ser563, and Ser566 on the outer surface of its  $\alpha$  helix, and Asn569 penultimate to its C terminus) from the secretin peptide.

In parallel, the motions of MxiM $^{28-142}$  were examined by  $^{15}\text{N}$  relaxation measurements. Consistent with its monomeric structure, the effective correlation time for the global tumbling of MxiM $^{28-142}$  derived from these data was 10.3 ns at 15°C. Although this increased slightly to 10.5 ns upon binding the small MxiD $^{553-570}$  peptide, no significant changes in the local backbone motions of the protein were detected (data not shown). In both states, the N and C termini of MxiM $^{28-142}$  were flexible on a subnanosecond time scale. This is also reflected by their high rms deviations in the NMR-derived ensemble of the protein (Figure 4) and the absence of detectable electron density for residues 28–32 in the crystal structure of the free pilot. Otherwise, the main chain amides of MxiM $^{28-142}$  were well ordered on this fast time scale, including throughout loop regions. Model-free analysis of the relaxation data yielded average general order parameters,  $S^2$ , of  $0.91 \pm 0.02$  and  $0.94 \pm 0.02$  for residues 34–140 of MxiM $^{28-142}$  in its peptide-free and -bound states, respectively. One notable exception is that, in both the absence and presence of MxiD $^{553-570}$ ,  $^{15}\text{N}$ -HSQC signals were not detected for MxiM $^{28-142}$  amides in the 119–126 region, suggestive of conformational exchange broadening on a millisecond-to-microsecond time scale. These residues form the exposed, mobile loop (L5) that extends above the open end of the barrel (Lario et al., 2005).

are very sensitive indicators of structural perturbations, and thus, while the former would be expected due to MxiD $^{553-570}$  binding at the interface, the latter extensive changes in the hydrophobic cavity were initially surprising.

A close comparison of the NMR-derived structure of the MxiM $^{28-142}$ -MxiD $^{553-570}$  complex and the crystal structure of free MxiM $^{28-142}$  revealed significant differences in the packing of aromatic side chains within the cavity. Specifically, upon peptide binding, the side chain dihedral angles of Trp54 changed such that its indole ring rotated to point its  $\text{N}^{\epsilon 1}\text{H}$  into the aromatic ring of Phe56, which concomitantly shifted from being “along side” to more “perpendicular across” the hydrophobic cavity (Figure 5C). This interaction, which structurally appears to be an NH-aromatic hydrogen bond (Steiner and Koellner, 2001), resulted in the dramatically upfield ring current-shifted  $^{15}\text{N}^{\epsilon 1}\text{H}$  signal of Trp54 from a typical value of  $\sim 10$  ppm to 5.52 ppm in the complex (Figure 3). In the absence of MxiD $^{553-570}$ , this indole signal was not detected, suggestive of conformational exchange broadening, and thus motions of the Trp54 side chain on the millisecond-to-microsecond time scale. Importantly, by rotating across the top of the hydrophobic cavity, Phe56 forms a platform to directly contact MxiD $^{553-570}$ . This suggests a possible mechanism for linking peptide binding on the surface of MxiM $^{28-142}$  to structural (and hence spectral) changes for residues within the hydrophobic cavity. Moreover, in the crystallographic structure of free MxiM $^{28-142}$ , electron density indicative of a bound alkyl chain was also observed within the cavity. In this case, the aromatic chains of Trp54 and Phe56 pointed in opposite directions to form the wall of the binding site. This raised the critical question as to whether or not a bound detergent or lipid was present in MxiM $^{28-142}$  or the MxiM $^{28-142}$ -MxiD $^{553-570}$  complex in solution.

Inspection of the  $\omega 1$ -filtered  $\omega 3$ -edited NOESY-HSQC spectra of  $^{15}\text{N}/^{13}\text{C}$ -labeled MxiM $^{28-142}$  revealed several NOE

**Table 1. NMR Restraints and Structural Statistics for the MxiM<sup>28–142</sup>/MxiD<sup>553–570</sup> Ensemble**

Summary of restraints				
No. of unambiguous (ambiguous) NOE restraints	MxiM	MxiD	Interface	Total
Intraresidue	950 (96)	116 (10)		1066 (106)
Sequential	433 (73)	87 (13)		520 (86)
Medium range (1 <  i – j  < 5)	251 (96)	78 (21)		329 (117)
Long range ( i – j  > 5)	613 (182)	35 (5)	86 (8)	734 (188)
Total	2248 (447)	316 (49)	86 (8)	2650 (497)
Dihedral angles (°)				
φ, ψ				86, 85
Deviation from restraints				
NOE restraints (Å)				0.055 ± 0.002
Dihedral angle restraints (°)				1.656 ± 0.117
Deviation from ideal geometry				
Bonds (Å)				(6.16 ± 0.15) × 10 <sup>-3</sup>
Angles (°)				0.75 ± 0.01
Improper angles (°)				1.96 ± 0.05
Residues in allowed regions of Ramachandran plot (%)				98.4 ± 0.76
Energies (kcal/mol)				
E <sub>bonds</sub>				82.7 ± 4.2
E <sub>angle</sub>				332 ± 9.5
E <sub>improper</sub>				154 ± 7.9
E <sub>vdw</sub>				-268 ± 17
E <sub>NOE</sub>				466 ± 23
E <sub>cdih</sub>				15.1 ± 2.0
Rmsd from average structure (Å)			Backbone (N, C <sup>α</sup> , C <sup>β</sup> )	All Heavy Atoms
MxiM <sup>28–142</sup> all residues			0.66 ± 0.14	1.12 ± 0.16
MxiM <sup>28–142</sup> residues 38–118, 126–140			0.37 ± 0.07	0.83 ± 0.13
MxiD <sup>553–570</sup> all residues			0.33 ± 0.10	0.70 ± 0.17
MxiD <sup>553–570</sup> residues 557–570			0.21 ± 0.11	0.69 ± 0.19
Complex all residues			0.64 ± 0.13	1.08 ± 0.16
Complex residues 38–118, 126–140, 561–570			0.39 ± 0.07	0.85 ± 0.13

± represents standard deviation.

crosspeaks between an unlabeled species and the labeled protein (Figure 6). Based upon its chemical shifts, the unlabeled species was most likely decylmaltoside (DM), retained from the initial purification step of MxiM<sup>28–142</sup>. Accordingly, the NOE peaks were assigned tentatively to interactions between the methyl groups of Ile38, Leu107, Leu111, Val115, Ile128, Leu136, and Leu138 with the alkyl tail of DM, of Thr58, Leu117, and Ile126, with both its tail and head group, and of Thr58 and Ile126, with its head group only. These residues line the wall and/or opening of the hydrophobic cavity (Figures 5A and 5B). Thus, consistent with previous X-ray crystallography and ITC measurements, NMR spectroscopy also reveals that MxiM<sup>28–142</sup> binds the alkyl chains from lipids and detergents within its hydrophobic cavity.

Given the affinity of the pilot protein for hydrocarbon chains, the exact compositions of the MxiM<sup>28–142</sup> samples used for structural analyses were not well defined. Indeed, the <sup>15</sup>N-HSQC spectra of the free protein showed considerable variation between samples, indicative of differing amounts of copurifying compounds. Efforts were made to prepare MxiM<sup>28–142</sup> under denaturing conditions to remove any potential hydrocar-

bons remaining from *E. coli*. However, only insoluble protein aggregates were obtained when the protein was transferred to a refolding buffer. This heterogeneity was improved by the addition of a small amount of DM detergent (below its CMC), allowing an NMR analysis of the peptide-free protein.

In contrast to free MxiM<sup>28–142</sup>, the NMR spectra of the MxiM<sup>28–142</sup>-MxiD<sup>553–570</sup> complex remained constant between samples. Furthermore, no NOE interactions with any DM could be detected (Figure 6). However, such interactions may not be observable due to several factors, including conformational exchange broadening or partial occupancy. Thus, we used commercially available <sup>13</sup>C<sub>16</sub>-labeled palmitic acid as a model compound to probe this potential interaction by NMR spectroscopy. In the X-ray crystal structure of MxiM<sup>28–142</sup>, the last two carbons of the bound alkyl chain are situated under the plane of the Trp54 indole, and would be expected to have upfield-shifted NMR signals due to an aromatic ring current effect. Indeed, in the constant-time <sup>13</sup>C-HSQC spectrum of <sup>13</sup>C<sub>16</sub>-palmitic acid mixed with MxiM<sup>28–142</sup>, <sup>1</sup>H signals from -<sup>13</sup>CH<sub>2</sub> and -<sup>13</sup>CH<sub>3</sub> groups were detected at 0.20 and -0.24

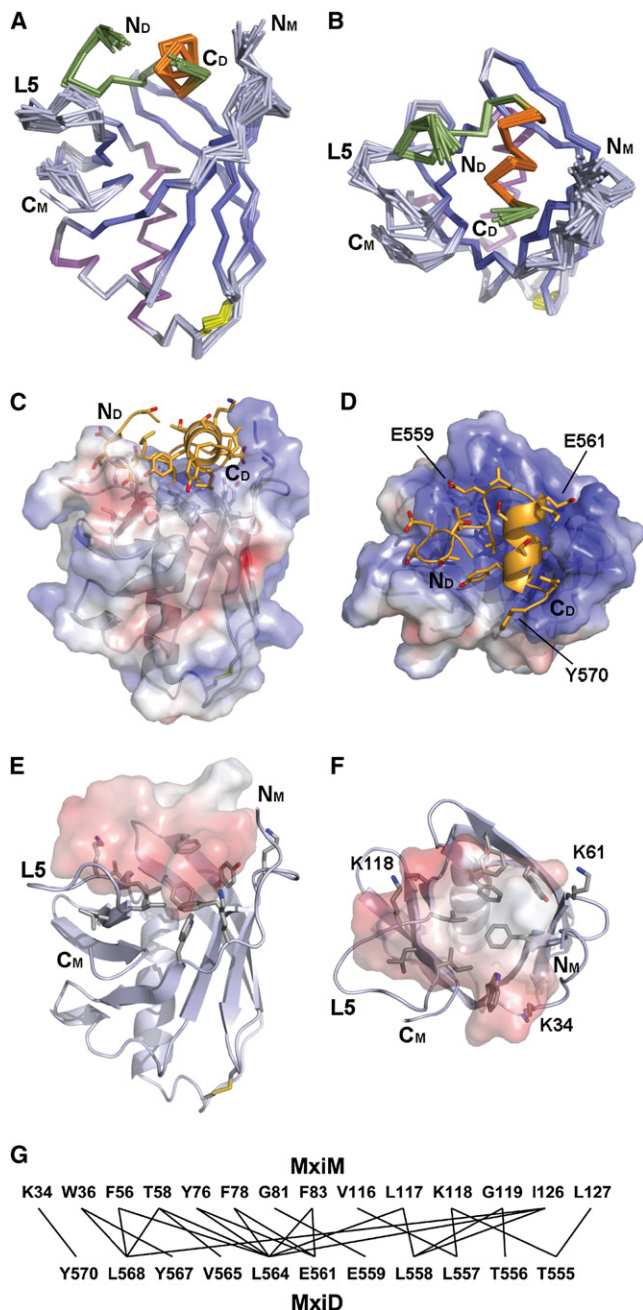


**Figure 4. The NMR-Derived Structure of the MxiM<sup>28-142</sup>/MxiD<sup>553-570</sup> Complex**

Shown are (A) “side-on” and (B) “top-down” backbone views of the superimposed ensemble, color coded to distinguish components and secondary structural elements (MxiM<sup>28-142</sup> bluish with a yellow disulfide; MxiD<sup>553-570</sup> green and orange). Also shown are views of a low-energy ensemble member highlighting all side chains of MxiD<sup>553-570</sup> (C and D) and the interfacial side chains of MxiM<sup>28-142</sup> (E and F) (oxygen, red; nitrogen, blue).

(C–F) In the latter four panels, the surface representations are for the corresponding partner of the complex, colored by electrostatic potential (negative, red; positive, blue) as calculated with APBS (Baker et al., 2001) and PyMol (DeLano, 2002). For clarity, only the surface and not the ribbon diagram of MxiD<sup>553-570</sup> is presented in (E and F). Residues forming intermolecular salt bridges, as well as loop L5 and the N and C termini of each member of the complex, are labeled. A close-up view of the interface is provided in Figure S1. The

ppm, respectively (Figure 7). These are ~1 ppm upfield from their unperturbed chemical shifts (1.25 and 0.83 ppm) in the absence of any protein. Upon adding MxiD<sup>553-570</sup>, only the latter signals from free palmitic acid were detected. We also measured long acquisition time <sup>13</sup>C-HSQC spectra of MxiM<sup>28-142</sup> in the presence of unlabeled DM (Figure 7). Again, a natural abundance signal from a methyl group was detected at 0.68 ppm in <sup>1</sup>H. The shift of this group is only 0.14 ppm upfield from that of free DM, possibly due to a different putative interaction with Trp54 or fast exchange with unbound detergent. Regardless, the signal was absent in the presence of MxiD<sup>553-570</sup>. Thus, both filtered-edited NOESY and <sup>13</sup>C-HSQC measurements demonstrate that MxiM<sup>28-142</sup> can bind the alkyl chain of DM or palmitic acid within its hydrophobic cavity, and this binding is abrogated upon complex formation with MxiD<sup>553-570</sup>.

## DISCUSSION

### General Features of a Pilot-Secretin Complex

This work presents what is, to our knowledge, the first structural description of a secretin-pilot complex. Upon binding its cognate pilot, the disordered C terminus of MxiD<sup>553-570</sup> folds into an amphipathic  $\alpha$  helix preceded by residues in an extended conformation. This helical peptide “lid” lies across the open end of the MxiM barrel, positioned by an extensive set of hydrophobic contacts, as well as three specific complimentary electrostatic interactions. Despite widespread spectral changes that are observed between the free and bound forms of MxiM, the overall cracked  $\beta$ -barrel fold is retained in both structures. However, there are key side chain rearrangements, highlighted by the repositioning of Trp54 and Phe56 within the MxiM lipid binding cavity, that likely have important functional implications for the pilot in its targeting of the secretin, MxiD, to the outer membrane.

MxiM binds alkyl chains within its hydrophobic cavity, as shown by X-ray crystallography, ITC, and now NMR spectroscopy. Importantly, we also demonstrated through NMR chemical shift and <sup>1</sup>H-<sup>1</sup>H NOE measurements that, upon MxiD binding, lipids are no longer detectable within this cavity. ITC data also confirm that saturating quantities of MxiD effectively preclude the lipid binding by MxiM (Lario et al., 2005). This results through two avenues. First, the MxiD helical lid sterically blocks access to the MxiM cavity, and second, the conformational rearrangement of the aromatic side chains of Trp54 and Phe56 to form the MxiD binding interface is incompatible with the presence of alkyl chains within the cavity. As will be elaborated below, a simple model for the biological function of MxiM can be extrapolated from the observation that the pilot can bind either a lipid chain or the secretin peptide in a mutually exclusive manner (Figure 8).

Will the interactions we observe between MxiM and MxiD be conserved in other pilotin/secretin complexes? In terms of the secretin components, secondary structure analyses of the C-terminal residues of several species, including the T3SS MxiD, YscC, OutD, and InvG, and the T2SS PulD, predict helical propensity, as observed herein for MxiD<sup>553-570</sup>. In terms of the

intermolecular <sup>1</sup>H-<sup>1</sup>H NOE connections defining the interface are summarized by lines in (G).

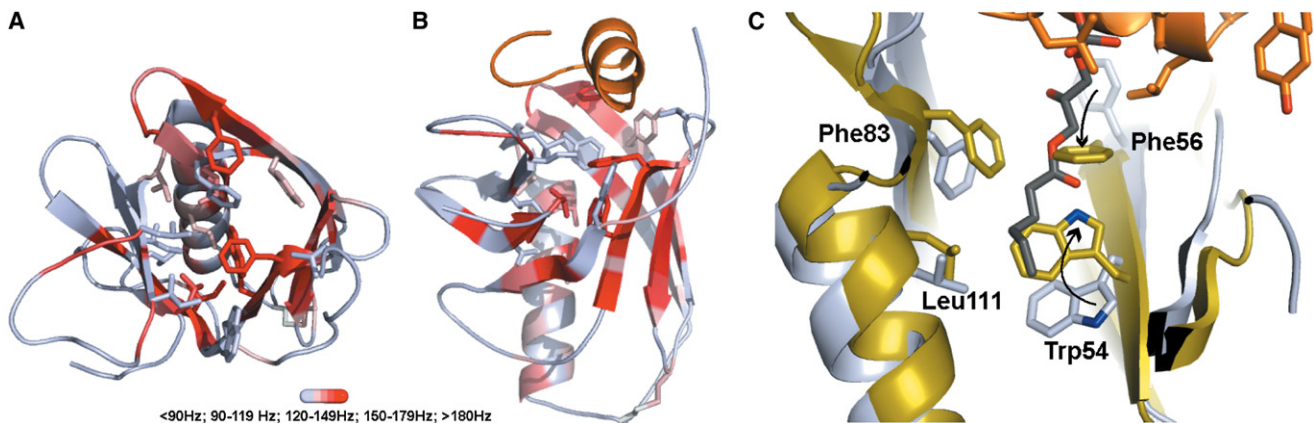


**Figure 5. Conformational Changes in MxiM<sup>28-142</sup> upon Binding MxiD<sup>553-570</sup>**

(A and B) Binding of MxiD<sup>553-570</sup> extensively perturbs the NMR spectra of MxiM<sup>28-142</sup> due to formation of a protein-peptide interface at the open end of the MxiM barrel and displacement of DM from its hydrophobic cavity. Mapped onto the backbone structure of the MxiM<sup>28-142</sup>/MxiD<sup>553-570</sup> complex ([A] top-down view with the peptide removed for clarity; [B] side-on view) are the rmsd changes in the available <sup>1</sup>H<sup>N</sup>, <sup>15</sup>N, <sup>13</sup>C<sup>α</sup>, <sup>13</sup>C<sup>γ</sup>, and/or indole <sup>1</sup>H<sup>ε1</sup> chemical shifts of MxiM<sup>28-142</sup> in the presence versus the absence of MxiD<sup>553-570</sup> (color gradient: white, <90 Hz; 90–119 Hz; 120–149 Hz; 150–179 Hz; red, >180 Hz, recorded with a 600 MHz NMR spectrometer). Note that no signals were detected for residues 120–124 in the L5 loop flanking the MxiD binding site. Also shown are the side chains of MxiM<sup>28-142</sup> that exhibited NOE interactions with bound DM in the absence of the secretin peptide.

(C) Superimposition of the side chains (oxygen, red; nitrogen, blue) forming the hydrophobic core of MxiM<sup>28-142</sup> in complex with 1-monoheptanoyl-2-hydroxyl-sn-glycerol-3-phosphate (1Y9T.PDB protein, gray; acyl chain, dark gray; Lario et al., 2005) and bound to MxiD<sup>553-570</sup> (protein, gold; peptide, orange). Phe56 and Trp54 are either separated to form a wall along the hydrophobic cavity for DM binding, or shifted together to form the base of the MxiD<sup>553-570</sup> binding site.

pilot components, this is more difficult to judge, as these lipoproteins share no detectable sequence similarity, and secondary structure predictions suggest helical propensity in some and  $\beta$ -strand propensity in others (the latter being verified for *Shigella* MxiM<sup>28-142</sup> [Lario et al., 2005]). Furthermore, it is likely that some pilots form additional contacts with distinct portions of their cognate secretins (Burghout et al., 2004a). However, in terms of secretin binding proteins in general, the features we observe in the MxiD-MxiM complex may also play functional roles in other systems. For example, the type-IV pilus *Neisseria* PilP exhibits a similar  $\beta$ -barrel architecture to MxiM, encompassing an extended hydrophobic cavity with an opening at one end of the barrel (Golovanov et al., 2006). Recent evidence suggests that binding of PilP to its cognate secretin PilQ is for the purpose of regulating pilus assembly rather than secretin localization (Balasingham et al., 2007). The latter role is attributed to a distinct lipoprotein PilW, which is composed of tetratricopeptide repeats, and thus bares no resemblance to MxiM (Trindade et al., 2008).

#### Similarities to the Lol Pathway and Lipocalins

Intriguingly, the T3SS pilot MxiM shares significant structural features with other lipid binding proteins, known as lipocalins, including LolA, LolB, and PagP (Figure S2; Lario et al., 2005). LolA and LolB have a fold that also binds acyl chains within a deep hydrophobic cavity of an unclosed  $\beta$  barrel (Takeda et al., 2003). These proteins function to sort lipoproteins for subsequent transport across the periplasm to the outer membrane (Figure 8). In a striking analogy to the intermolecular MxiD-MxiM complex, LolA also requires the displacement of intramolecular lid helices prior to binding the acyl chain of a lipidated protein within its hydrophobic cavity (Takeda et al., 2003). When the lid is in its closed conformation, no lipid is bound, as demonstrated by the crystallographically determined structure of this protein at

1.6 Å resolution (Takeda et al., 2003). The N-terminal helix of LolA lies perpendicular across its lipid binding cavity in an orientation similar to that observed for the C-terminal helix of MxiD, which blocks the lipid binding cavity of MxiM (Figure S2). Furthermore, MxiM and LolA both function in shuttling proteins to the outer membrane. Thus, the positioning of a helical lid across a  $\beta$  barrel to occlude lipid binding may reflect common evolutionary features of a T3SS pilot/secretin pair and the Lol pathway transporters.

#### A Model for the Function of MxiM

Common to the T2SS, T3SS, and type-IV pili is the observation that proper targeting of the secretin ring to the outer membrane requires the presence of a lipidated pilot protein (Schuch and Maurelli, 2001; Guilvout et al., 2006). Based upon our current structural and thermodynamic demonstration of mutually exclusive binding of lipids and MxiD to MxiM, combined with studies of related systems, we propose a model of pilot-mediated targeting that is summarized in Figure 8. Independent of the secretin, the pilot is constitutively expressed (D'Enfert and Pugsley, 1989) and secreted across the inner membrane. The periplasmic MxiM will be N-terminally lipidated, because it possesses the classic lipidation LxGC sequence motif at its secretory leader cleavage site. Furthermore, the absence of an Asp residue following the modified Cys in the lipidation motif allows targeting of the pilot to the outer membrane by the Lol sorting pathway (Yamaguchi et al., 1988; Terada et al., 2001). Indeed, localization studies have shown that a proportion of pilot proteins, including MxiM, are embedded in the outer membrane, presumably by virtue of a covalently attached lipid (Daefler and Russel, 1998; Shevchik and Condemine, 1998; Schuch and Maurelli, 1999). If, as previous data suggest (Guilvout et al., 2006; Collin et al., 2007), one of the primary roles of the pilot is to target the secretin

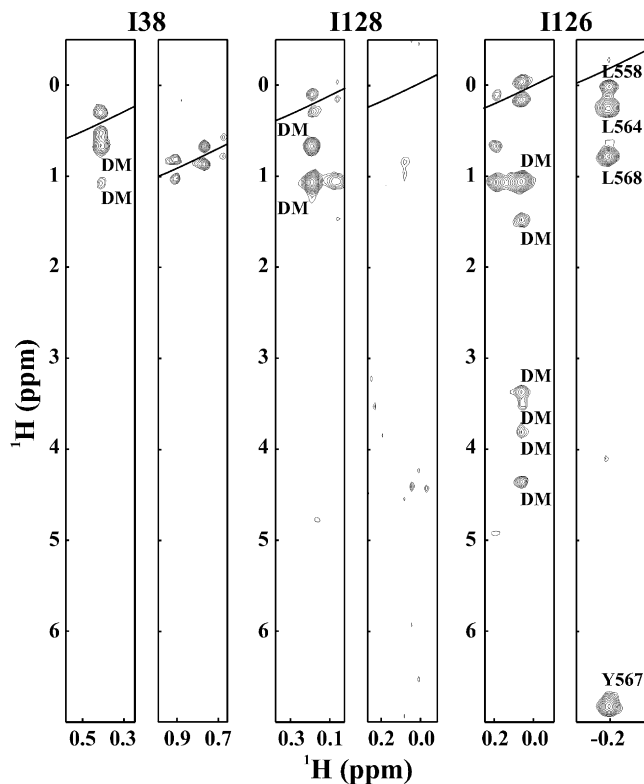


**Figure 6. MxiM<sup>28-142</sup> Binds DM Only in the Absence of MxiD<sup>553-570</sup>**

Shown are  $^1\text{H}$ - $^1\text{H}$  strips from  $\omega_1$ -filtered  $\omega_3$ -edited NOESY-HSQC spectra of  $^{13}\text{C}$ -labeled MxiM<sup>28-142</sup> in the absence (left) and presence (right) of unlabeled MxiD<sup>553-570</sup>, taken at the  $^{13}\text{C}$  chemical shifts of the  $\delta^1$  methyl groups from I38, I128, and I126. NOE crosspeaks, which only arise between close (<5 Å) protons on the unlabeled ligand and  $^{13}\text{C}$ -labeled protein, are assigned to DM or to specific residues from MxiD<sup>553-570</sup>. I126 exhibits several NOE interactions to either DM or MxiD<sup>553-570</sup>, whereas I38 and I128 only interact with DM. Incompletely suppressed diagonal peaks appear as  $^{13}\text{C}$ -coupled doublets along the positions indicated by the sloping line.

appropriately to the outer membrane, then this raises the key question of how the lipidated pilot can make contact with the nascent chain of its cognate secretin before its own Lol-mediated transfer. A feasible answer lies with the observation that the binding of LolA to lipoproteins is relatively weak, principally to allow their subsequent transfer to its partner outer-membrane protein, LolB, which has a much higher affinity for lipids (Matsuyama et al., 1997). Thus, we hypothesize that an equilibrium exists in which MxiM binds the alkyl chain of its own N-terminal lipid within its hydrophobic cavity. This intramolecular interaction sequesters the lipid, thereby preventing the complete transfer of the pilot to the outer membrane via LolA-mediated passage to LolB. The net result of these competitive equilibria insures a sufficient periplasmic pool of the pilot for association with its secretin partner. Upon expression and secretion of the MxiD across the inner membrane, its unstructured C-terminal region can bind MxiM, inducing the turn-helix motif that we observe in the structure presented here that caps the hydrophobic cavity and induces a conformational rearrangement of the aromatic residues Trp54 and Tyr56 within MxiM's lipid binding site. The net result of complex formation is to shift the above equilibrium

distribution toward the state with the pilot's lipid exposed, while also indirectly preventing the membrane spanning secretin from being prematurely embedded in the inner membrane. The MxiM/MxiD complex is then sorted to the outer-membrane via binding of the pilot's lipidated N terminus to the Lol system (Narita et al., 2004; Terada et al., 2001). LolB facilitates the insertion of MxiM into the inner leaflet of the outer membrane, resulting in the localization of MxiD. This proposed model addresses the functional role of a lipidated pilot in passage of its cognate secretin across the periplasm to the outer membrane, where proper assembly of the secretin ring can occur.

The crucial interface between MxiM and MxiD from the *Shigella* T3SS illustrated in this work represents the first structural report of a secretin bound to its cognate pilot. Consideration of this complex in the context of the Lol system both strongly supports a role of MxiM as a transporter for the proper localization of the secretin in the outer membrane, and yields an attractive and testable model based on the displacement of a sequestered lipid chain upon MxiD binding. The interaction between the secretin and its pilot is essential for the proper assembly of the T3SS and transport of virulence factors from Gram-negative pathogenic bacteria into host cells. Therefore, this presents a clear target for inhibiting the formation of the T3SS and for the design of antimicrobials.

## EXPERIMENTAL PROCEDURES

### Synthetic Peptide

The N-acetylated peptide MxiD<sup>552-570</sup> (Ac-SETTLEDEKSLVSYLNY) was purchased from CS Bio Company, Inc.

### Expression and Purification of MxiM<sup>28-142</sup> and MxiD<sup>525-570</sup>

Initial attempts to study lipidated full-length MxiM *in vitro* were complicated by the aggregation of the purified protein. Since lipidation is important for membrane localization, but not for secretin interaction (Schuch and Maurelli, 2001), we used the soluble truncated pilot construct MxiM<sup>24-142</sup> for all the studies described here. Unlabeled His<sub>6</sub>-tagged MxiM<sup>24-142</sup> and His<sub>6</sub>-tagged MxiD<sup>525-570</sup> were expressed with pET28a and purified as described previously (Lario et al., 2005). Isotopically labeled samples were prepared with *E. coli* BL21 ( $\lambda$ DE3) grown at 37°C in M9 minimal medium containing 1g/L  $^{15}\text{NH}_4\text{Cl}$  and/or 3 g/L  $^{13}\text{C}_6$ -glucose. At an OD<sub>600</sub> of ~0.8, the cells were cooled to 20°C for 30 min, followed by induction of protein expression with 0.5 mM IPTG. After 14 hr, the cells were harvested by centrifugation and frozen at -80°C before purification by Ni<sup>2+</sup>-affinity chromatography. DM detergent was necessary to isolate His<sub>6</sub>-MxiM<sup>24-142</sup> from the membrane fraction, despite the lack of lipidation site on this construct. However, the protein remained soluble in subsequent detergentless buffer (buffer A: 20 mM PIPES, pH 7.0, and 50 mM NaCl). Unfortunately, despite several different unfolding-refolding strategies, as well as the use of Bio-beads (Bio-Rad) extraction, a completely detergent-free sample of MxiM<sup>24-142</sup> could not be obtained. During thrombin cleavage, the His<sub>6</sub>-MxiM<sup>24-142</sup> construct is further processed to yield MxiM<sup>28-142</sup> (Lario et al., 2005). After proteolytic cleavage of the His<sub>6</sub>-tag, MxiD<sup>525-570</sup> has the sequence, (GSHM)KESYYNTAEYKSLISEREIQKTTQIIPS ETTLEDEKSLVSYLNY, with the first four residues remaining from the expression system. The samples, confirmed by mass spectrometry, were adjusted to their final buffer conditions by ultrafiltration. Concentrations were determined by absorbance spectroscopy with a predicted molar extinction coefficient  $\epsilon_{280} = 15595 \text{ M}^{-1} \text{ cm}^{-1}$  for MxiM<sup>28-142</sup>,  $7450 \text{ M}^{-1} \text{ cm}^{-1}$  for MxiD<sup>525-570</sup>, and  $2980 \text{ M}^{-1} \text{ cm}^{-1}$  for MxiD<sup>552-570</sup> (<http://ca.expasy.org/tools/protparam.html>).

### NMR Spectroscopy

NMR spectra were recorded at 15°C on Varian Unity 500 and cryoprobe Inova 600 MHz NMR spectrometers. Unless noted otherwise, the samples consisted of 0.3–0.7 mM protein, peptide, or 1:1 protein:peptide complex in 20 mM

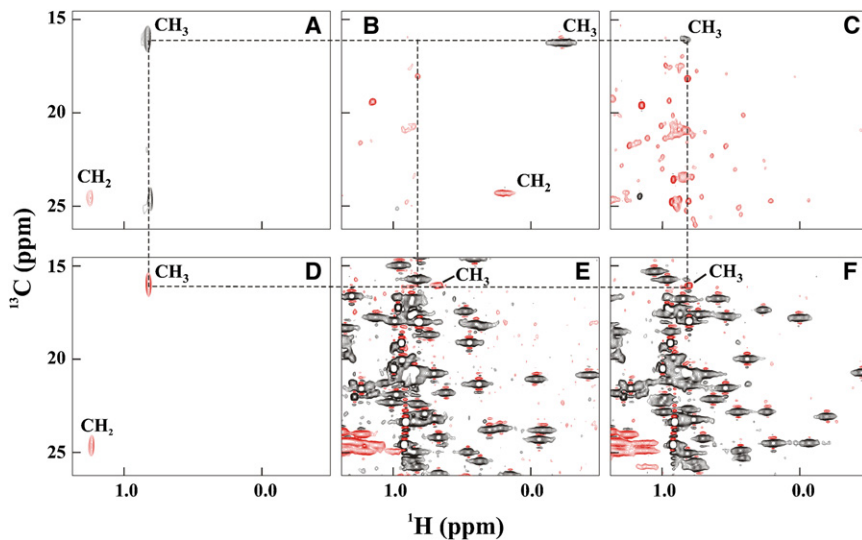


**Figure 7. MxiM<sup>553-570</sup> Excludes Binding of Palmitic Acid and DM by MxiM<sup>28-142</sup>**

Shown are portions of the constant time <sup>13</sup>C-HSQC spectra of <sup>13</sup>C<sub>16</sub>-palmitic acid in the (A) absence and presence of unlabeled (B) MxiM<sup>28-142</sup> and the (C) MxiM<sup>28-142</sup>/MxiD<sup>553-570</sup> complex (2.5 mM palmitic acid, 0.5 mM MxiM<sup>28-142</sup>, 1 mM MxiD<sup>553-570</sup>). Upfield-shifted signals in (A) are attributed to the terminal -<sup>13</sup>CH<sub>2</sub>-<sup>13</sup>CH<sub>3</sub> moiety of palmitic acid bound in the hydrophobic cavity of peptide-free MxiM<sup>28-142</sup> and adjacent to aromatic side chains. Note that signals from -CH<sub>3</sub> (black) and -CH<sub>2</sub>- (red) groups in <sup>13</sup>C<sub>16</sub>-palmitic acid have opposite signs in these constant-time spectra; the natural-abundance methyls in the unlabeled protein are red. Also shown are portions of the constant-time <sup>13</sup>C-HSQC spectra of unlabeled DM in the (D) absence and presence of <sup>13</sup>C-labeled (E) MxiM<sup>28-142</sup> and (F) the MxiM<sup>28-142</sup>/MxiD<sup>553-570</sup> complex (0.5 mM DM, 0.3 mM MxiM<sup>28-142</sup>, 0.4 mM MxiD<sup>553-570</sup>). The <sup>13</sup>C signals from DM (red) are detected at natural abundance and thus have the opposite sign from those of the <sup>13</sup>C-labeled methyl groups (black) in the protein. The dashed lines indicate the positions of the -CH<sub>3</sub> groups of free palmitic acid and DM.

HEPES, pH 6.5 or 7.5, 0.5 mM DM, and ~5% D<sub>2</sub>O. The reduced temperature was used to limit aggregation. Signals from the <sup>1</sup>H, <sup>13</sup>C, and <sup>15</sup>N nuclei of <sup>13</sup>C/<sup>15</sup>N-labeled MxiD<sup>525-570</sup> (free and bound to unlabeled MxiM<sup>28-142</sup>) and of <sup>13</sup>C/<sup>15</sup>N-labeled MxiM<sup>28-142</sup> (free and in complex with unlabeled MxiD<sup>553-570</sup>) were detected and assigned by standard NMR experiments (Sattler et al., 1999). The <sup>1</sup>H signals of unlabeled MxiM<sup>553-570</sup> bound to uniformly <sup>13</sup>C/<sup>15</sup>N-labeled MxiM<sup>28-142</sup> were assigned via <sup>13</sup>C/<sup>15</sup>N ω<sub>1</sub>,ω<sub>2</sub>-filtered TOCSY and NOESY spectra (Ikura and Bax, 1992). The binding of DM and <sup>13</sup>C-palmitic acid (Spectra Stable Isotopes) to MxiM<sup>28-142</sup> was monitored with constant-time <sup>13</sup>C-HSQC and <sup>13</sup>C/<sup>15</sup>N ω<sub>1</sub>-filtered ω<sub>3</sub>-edited NOESY-HSQC measurements (Zwahlen et al., 1997). The NMR data were processed with NMRPipe (Delaglio et al., 1995) and analyzed in NMRView (Johnson and Blevins, 1994). <sup>15</sup>N T<sub>1</sub>, T<sub>2</sub>, and heteronuclear NOE relaxation experiments were fit with Tensor2 (Dosset et al., 2000).

The chemical shift assignments of MxiM<sup>28-142</sup>, MxiD<sup>525-570</sup>, MxiD<sup>553-570</sup> bound to MxiM<sup>28-142</sup>, and the MxiM<sup>28-142</sup>-MxiD<sup>553-570</sup> complex have been

deposited in the BioMagResBank (<http://www.bmrb.wisc.edu/>) under accession codes 15503, 15497, 7407, and 15504, respectively.

#### Structure Calculations

The MxiM<sup>28-142</sup>/MxiD<sup>553-570</sup> complex structure was calculated with ARIA v2.1 (Nilges, 1995) and CNS v1.1 (Brünger et al., 1998), as summarized in Table 1. A proton chemical shift refinement protocol (Kuszewski et al., 1995) was implemented in ARIA. Distance restraints were derived from a simultaneous 3D <sup>13</sup>C/<sup>15</sup>N-edited NOESY-HSQC (Zwahlen et al., 1998) (intra- and intermolecular NOEs to MxiM<sup>28-142</sup>, τ<sub>mix</sub> = 100 ms), 2D and 3D <sup>13</sup>C/<sup>15</sup>N ω<sub>1</sub>-filtered ω<sub>3</sub>-edited NOESY-HSQC (Zwahlen et al., 1997) (only intermolecular NOEs, 150 ms), and 2D <sup>13</sup>C/<sup>15</sup>N ω<sub>1</sub>,ω<sub>2</sub>-filtered NOESY spectra (Ikura and Bax, 1992) (only intramolecular MxiD<sup>553-570</sup> NOEs, 150 ms) spectra of <sup>13</sup>C/<sup>15</sup>N-MxiM<sup>28-142</sup> bound to unlabeled MxiD<sup>553-570</sup>. All intermolecular MxiM/MxiD NOE signals were assigned manually, whereas the majority of intramolecular NOE signals were assigned automatically by ARIA. Backbone dihedral angles were predicted

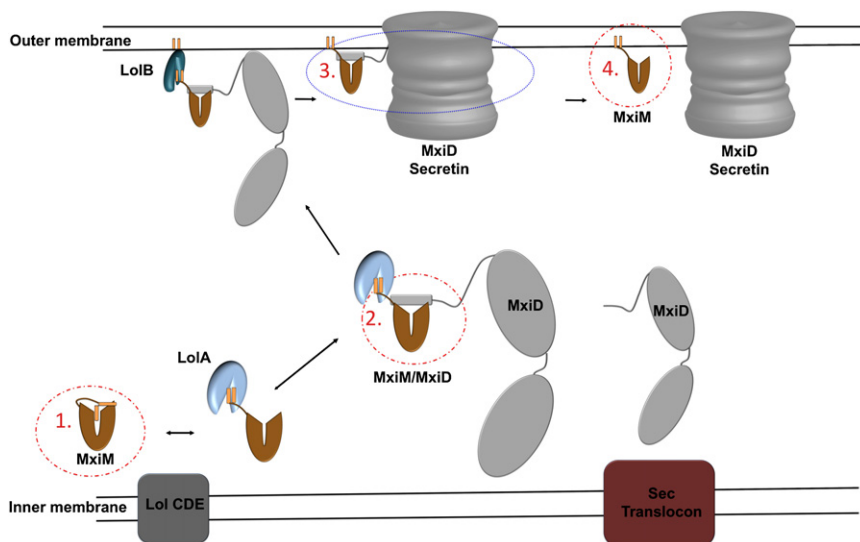


**Figure 8. A Model of Translocation of MxiM and MxiD to the Outer Membrane via the Lol Pathway**

Highlighted circles represent stages that are supported by direct experimental evidence (red) or by evidence from homologous systems (blue). (1) MxiM with its lipid acyl chains sequestered intramolecularly (Lario et al., 2005). (2) MxiM bound to the C terminus of MxiD (complex structure presented herein), with lipids accessible for LolA-mediated transport. (3) MxiM bound to the oligomerized secretin, as supported by an electron micrograph of PulS-bound PulD (Nouwen et al., 1999). (4) MxiM localized to the inner leaflet of the outer membrane of *Shigella* (Schuch and Maurelli, 1999) (see Discussion).

by TALOS (Cornilescu et al., 1999). A disulfide bond between Cys69 and Cys95 was introduced based upon their  $^{13}\text{C}^{\beta}$  chemical shifts (diagnostic of the oxidized state) and their close juxtapositioning by NOE interactions.

The coordinates of the MxiM<sup>28–142</sup>/MxiD<sup>553–570</sup> ensemble have been deposited in the Research Collaboratory for Structural Bioinformatics Protein Databank (2JW1; <http://www.rcsb.org/pdb/>).

### ITC

ITC was performed with a VP ITC (MicroCal, Inc., Northampton MA). All samples were pH 7.5 in 20 mM HEPES. Titrations were performed by injecting 25 consecutive 10  $\mu\text{l}$  aliquots of 130  $\mu\text{M}$  MxiD<sup>553–570</sup> into the ITC cell (volume = 1.3528 ml) containing 12.2  $\mu\text{M}$  MxiM<sup>28–142</sup>. The ITC data were corrected for the heat of dilution of the titrant by subtracting mixing enthalpies for 10  $\mu\text{l}$  injections of MxiD<sup>553–570</sup> into protein-free buffer. Binding stoichiometry, enthalpy, and equilibrium association constants were determined by fitting the corrected data to a bimolecular interaction model.

### SUPPLEMENTAL DATA

Supplemental Data include two figures and Supplemental References and can be found with this article online at <http://www.structure.org/cgi/content/full/16/10/1544/DC1/>.

### ACKNOWLEDGMENTS

We thank Lewis Kay for providing NMR pulse sequences, Young Mee Tiffany Jung for assistance with ITC, and Thomas Spreter for valuable discussions. This research was funded by the Canada Foundation for Innovation, the British Columbia Knowledge Development Fund, the UBC Blusson Fund, the Michael Smith Foundation for Health Research (MSFHR), and the Canadian Institutes of Health Research (CIHR). P.L. and T.F.M. were supported by MSFHR post-doctoral fellowships. N.C.J.S. is an MSFHR Senior Scholar, CIHR Investigator, and Howard Hughes Medical Institute International Scholar. L.P.M. gratefully acknowledges the sabbatical support of a Killam Faculty Research Fellowship, a Séjour Scientifique de Haut Niveau Award from the French Embassy in Canada, and a CIHR-Centre National de la Recherche Scientifique International Exchange grant.

Received: June 14, 2008

Revised: August 8, 2008

Accepted: August 15, 2008

Published: October 7, 2008

### REFERENCES

Ahn, V.E., Lo, E.I., Engel, C.K., Chen, L., Hwang, P.M., Kay, L.E., Bishop, R.E., and Privé, G.G. (2004). A hydrocarbon ruler measures palmitate in the enzymatic acylation of endotoxin. *EMBO J.* 23, 2931–2941.

Allaoui, A., Sansonetti, P.J., and Parsot, C. (1992). MxiJ, a lipoprotein involved in secretion of *Shigella* lpa invasins, is homologous to YscJ, a secretion factor of the *Yersinia* Yop proteins. *J. Bacteriol.* 174, 7661–7669.

Baker, N.A., Sept, D., Joseph, S., Holst, M.J., and McCammon, J.A. (2001). Electrostatics of nanosystems, application to microtubules and the ribosome. *Proc. Natl. Acad. Sci. USA* 98, 10037–10041.

Balasingham, S.V., Collins, R.F., Assalkhou, R., Homberset, H., Frye, S.A., Derrick, J.P., and Tønnum, T. (2007). Interactions between the lipoprotein PilP and the secretin PilQ in *Neisseria meningitidis*. *J. Bacteriol.* 189, 5716–5727.

Blocker, A., Jouihri, N., Larquet, E., Gounon, P., Ebel, F., Parsot, C., Sansonetti, P., and Allaoui, A. (2001). Structure and composition of the *Shigella flexneri* "needle complex", a part of its type III secretin. *Mol. Microbiol.* 39, 652–663.

Brünger, A.T., Adams, P.D., Clore, G.M., DeLano, W.L., Gros, P., Grosse-Kunstleve, R.W., Jiang, J.S., Kuszewski, J., Nilges, M., Pannu, N.S., et al. (1998). Crystallography & NMR system. A new software suite for macromolecular structure determination. *Acta Crystallogr. D Biol. Crystallogr.* 54, 905–921.

Burghout, P., Beckers, F., de Wit, E., van Boxtel, R., Cornelis, G.R., Tommassen, J., and Koster, M. (2004a). Role of the pilot protein YscW in the biogenesis of the YscC secretin in *Yersinia enterocolitica*. *J. Bacteriol.* 186, 5366–5375.

Burghout, P., van Boxtel, R., Van Gelder, P., Ringler, P., Müller, S.A., Tommassen, J., and Koster, M. (2004b). Structure and electrophysiological properties of the YscC secretin from the type III secretion system of *Yersinia enterocolitica*. *J. Bacteriol.* 186, 4645–4654.

Collin, S., Guilvout, I., Chami, M., and Pugsley, A.P. (2007). YaeT-independent multimerization and outer membrane association of secretin PulD. *Mol. Microbiol.* 64, 1350–1357.

Collins, R.F., Frye, S.A., Kitmitto, A., Ford, R.C., Tønnum, T., and Derrick, J.P. (2004). Structure of the *Neisseria meningitidis* outer membrane PilQ secretin complex at 12 Å resolution. *J. Biol. Chem.* 279, 39750–39756.

Cornilescu, G., Delaglio, F., and Bax, A. (1999). Protein backbone angle restraints from searching a database for chemical shift and sequence homology. *J. Biomol. NMR* 13, 289–302.

D'Enfert, C., and Pugsley, A.P. (1989). *Klebsiella pneumoniae* pulS gene encodes an outer membrane lipoprotein required for pullulanase secretion. *J. Bacteriol.* 171, 3673–3679.

Daefler, S., Guilvout, I., Hardie, K.R., Pugsley, A.P., and Russel, M. (1997). The C-terminal domain of the secretin PulD contains the binding site for its cognate chaperone, PulS, and confers PulS dependence on pilVf1 function. *Mol. Microbiol.* 24, 465–475.

Daefler, S., and Russel, M. (1998). The *Salmonella typhimurium* InvH protein is an outer membrane lipoprotein required for the proper localization of InvG. *Mol. Microbiol.* 28, 1367–1380.

Delaglio, F., Grzesiek, S., Vuister, G.W., Zhu, G., Pfeifer, J., and Bax, A. (1995). NMRPipe, a multidimensional spectral processing system based on UNIX pipes. *J. Biomol. NMR* 6, 277–293.

DeLano, W.L. (2002). The PyMOL Molecular Graphics System (Palo Alto, CA: DeLano Scientific).

Dosset, P., Hus, J.C., Blackledge, M., and Marion, D. (2000). Efficient analysis of macromolecular rotational diffusion from heteronuclear relaxation data. *J. Biomol. NMR* 16, 23–28.

Flower, D.R., North, A.C., and Sansom, C.E. (2000). The lipocalin protein family, structural and sequence overview. *Biochim. Biophys. Acta* 1482, 9–24.

Genin, S., and Boucher, C.A. (1994). A superfamily of proteins involved in different secretion pathways in gram-negative bacteria, modular structure and specificity of the N-terminal domain. *Mol. Gen. Genet.* 243, 112–118.

Golovanov, A.P., Balasingham, S., Tzitzilonis, C., Goult, B.T., Lian, L.Y., Homberset, H., Tønnum, T., and Derrick, J.P. (2006). The solution structure of a domain from the *Neisseria meningitidis* lipoprotein PilP reveals a new  $\beta$ -sandwich fold. *J. Mol. Biol.* 364, 186–195.

Guilvout, I., Chami, M., Engel, A., Pugsley, A.P., and Bayan, N. (2006). Bacterial outer membrane secretin PulD assembles and inserts into the inner membrane in the absence of its pilotin. *EMBO J.* 25, 5241–5249.

Hardie, K.R., Lory, S., and Pugsley, A.P. (1996). Insertion of an outer membrane protein in *Escherichia coli* requires a chaperone-like protein. *EMBO J.* 15, 978–988.

Hayashi, S., and Wu, H.C. (1990). Lipoproteins in bacteria. *J. Bioenerg. Biomembr.* 22, 451–471.

Johnson, B.A., and Blevins, R.A. (1994). NMR View: a computer program for the visualization and analysis of NMR data. *J. Biomol. NMR* 4, 603–614.

Ikura, M., and Bax, A. (1992). Isotope-filtered 2D NMR of a protein-peptide complex. Study of a skeletal muscle myosin light chain kinases fragment bound to calmodulin. *J. Am. Chem. Soc.* 114, 2433–2440.

Koster, M., Bitter, W., de Cock, H., Allaoui, A., Cornelis, G.R., and Tommassen, J. (1997). The outer membrane component, YscC, of the Yop secretion machinery of *Yersinia enterocolitica* forms a ring-shaped multimeric complex. *Mol. Microbiol.* 26, 789–797.

Kotloff, K.L., Winickoff, J.P., Ivanoff, B., Clemens, J.D., Swerdlow, D.L., Sansonetti, P.J., Adak, G.K., and Levine, M.M. (1999). Global burden of *Shigella* infections, implications for vaccine development and implementation of control strategies. *Bull. World Health Organ.* 77, 651–666.

- Kuszewski, J., Gronenborn, A.M., and Clore, G.M. (1995). The impact of direct refinement against proton chemical shifts on protein structure determination by NMR. *J. Magn. Reson. B*, *107B*, 293–297.
- Lario, P.I., Pfuetzner, R.A., Frey, E.A., Creagh, L., Haynes, C., Maurelli, A.T., and Strynadka, N.C.J. (2005). Structure and biochemical analysis of a secretin pilot protein. *EMBO J.* *24*, 1111–1121.
- Linderoth, N.A., Simon, M.N., and Russel, M. (1997). The filamentous phage pIV multimer visualized by scanning transmission electron microscopy. *Science* *278*, 1635–1638.
- Marsh, J.A., Singh, V.K., Jia, Z., and Forman-Kay, J.D. (2006). Sensitivity of secondary structure propensities to sequence differences between  $\alpha$ - and  $\gamma$ -synuclein, implications for fibrillation. *Protein Sci.* *15*, 2795–2804.
- Matsuyama, S., Yokota, N., and Tokuda, H. (1997). A novel outer membrane lipoprotein, LolB (HemM), involved in the LolA (p20)-dependent localization of lipoproteins to the outer membrane of *Escherichia coli*. *EMBO J.* *16*, 6947–6955.
- Narita, S., Matsuyama, S., and Tokuda, H. (2004). Lipoprotein trafficking in *Escherichia coli*. *Arch. Microbiol.* *182*, 1–6.
- Nilges, M. (1995). Calculation of protein structures with ambiguous distance restraints, automated assignment of ambiguous NOE crosspeaks and disulphide connectivities. *J. Mol. Biol.* *245*, 645–660.
- Nouwen, N., Ranson, N., Saibil, H., Wolpensinger, B., Engel, A., Ghazi, A., and Pugsley, A.P. (1999). Secretin PulD, association with pilot PulS, structure, and ion-conducting channel formation. *Proc. Natl. Acad. Sci. USA* *96*, 8173–8177.
- Sattler, M., Schleucher, J., and Griesinger, C. (1999). Heteronuclear multidimensional NMR experiments for the structure determination of proteins in solution employing pulsed field gradients. *Prog. NMR Spectrosc.* *34*, 93–158.
- Schuch, R., and Maurelli, A.T. (1999). The Mxi-Spa type III secretory pathway of *Shigella flexneri* requires an outer membrane lipoprotein, MxiM, for invasive translocation. *Infect. Immun.* *67*, 1982–1991.
- Schuch, R., and Maurelli, A.T. (2001). MxiM and MxiJ, base elements of the Mxi-Spa type III secretion system of *Shigella*, interact with and stabilize the MxiD secretin in the cell envelope. *J. Bacteriol.* *183*, 6991–6998.
- Shevchik, V.E., and Condemine, G. (1998). Functional characterization of the *Erwinia chrysanthemi* OutS protein, an element of a type II secretion system. *Microbiology* *144*, 3219–3228.
- Steiner, T., and Koellner, G. (2001). Hydrogen bonds with  $\pi$ -acceptors in proteins: frequencies and role in stabilizing local 3D structures. *J. Mol. Biol.* *305*, 535–557.
- Takeda, K., Miyatake, H., Yokota, N., Matsuyama, S., Tokuda, H., and Miki, K. (2003). Crystal structures of bacterial lipoprotein localization factors, LolA and LolB. *EMBO J.* *22*, 3199–3209.
- Terada, M., Kuroda, T., Matsuyama, S., and Tokuda, H. (2001). Lipoprotein sorting signals evaluated as the LolA-dependent release of lipoproteins from the cytoplasmic membrane of *Escherichia coli*. *J. Biol. Chem.* *276*, 47690–47694.
- Thanassi, D.G., and Hultgren, S.J. (2000). Multiple pathways allow protein secretion across the bacterial outer membrane. *Curr. Opin. Cell Biol.* *12*, 420–430.
- Trindade, M.B., Job, V., Contreras-Martel, C., Pelicic, V., and Dessen, A. (2008). Structure of a widely conserved type IV pilus biogenesis factor that affects the stability of secretin multimers. *J. Mol. Biol.* *378*, 1031–1039.
- Yamaguchi, K., Yu, F., and Inouye, M. (1988). A single amino acid determinant of the membrane localization of lipoproteins in *E. coli*. *Cell* *53*, 423–432.
- Zwahlen, C., Gardner, K.H., Sarma, S.P., Horita, D.A., Byrd, R.A., and Kay, L.E. (1998). An NMR experiment for measuring methyl-methyl NOEs in <sup>13</sup>C-labeled proteins with high resolution. *J. Am. Chem. Soc.* *120*, 7617–7625.
- Zwahlen, C., Legault, P., Vincent, S.J.F., Greenblatt, J., Konrat, R., and Kay, L.E. (1997). Methods for measurement of intermolecular NOEs by multinuclear NMR spectroscopy: application to a bacteriophage N-Peptide/boxB RNA complex. *J. Am. Chem. Soc.* *119*, 6711–6721.